JMEPEG (2012) 21:2117–2123
DOI: 10.1007/s11665-012-0138-y

1059-9495/$19.00

Impact Toughness of an Isothermally Treated Zeron®100 SDSS

Irene Calliari, Marco Breda, Emilio Ramous, Katya Brunelli, Marco Pizzo, and Cinzia Menapace

(Submitted June 15, 2011; in revised form December 19, 2011)

The aim of the present study is to investigate the impact toughness of a UNS 32760 SDSS, in relation to the quantity of secondary phases precipitated after isothermal aging in the range of 850-950 °C and for different exposure times. The impact toughness has been investigated by means of instrumented impact testing, using Charpy V-notched specimens at room temperature. The impact testing results show that, for an amount of about 0.5% volume fraction of intermetallic phase, the impact toughness is reduced by over 50%. For volume fractions higher than 1.5-2%, the impact toughness is definitively compromised, and small entities of plastic deformations are enough to cause a prevailing brittle fracture mechanism. By increasing the precipitates' amounts, the fracture mechanism shows an ever more prominent brittle behavior until 6% volume fraction, exceeding which the ductile component is totally absent.

Keywords chi phase, duplex stainless steel, impact toughness, isothermal aging, sigma phase, Zeron®100

1. Introduction

Duplex stainless steels (DSS) may be defined as a category of steels having a two-phase ferritic-austenitic microstructure, where the phases are present in relatively large separate volumes and in approximately equal volume fractions (Ref 1). In general, these alloys have two or three times higher yield strength than the austenitic grades and exhibit resistance to localized and stress corrosion in many corrosive environments comparable or superior to that of austenitic steels containing comparable additions of chromium and molybdenum (Ref 2). These steels combine good mechanical and corrosion properties; however, due both to the large amount of alloying element content and to the instability of the ferritic matrix at the high temperatures, they are susceptible to the formation of dangerous intermetallic phases, such as σ and χ phases, after aging the material at a temperature >600 °C (Ref 1).

The resistance to corrosion depends on chemical composition and microstructure. The composition mainly influences the resistance to pitting corrosion; thus elements like chromium, molybdenum, tungsten, and nitrogen improve this feature, whereas the resistance to stress corrosion can be improved by increasing the volume fraction of ferrite (Ref 1). The presence of intermetallic phases reduces the volume fraction of the ferritic phase and depletes the matrix in elements that enhance the corrosion resistance, making these steels not resistant any more.

While the tensile properties of DSS were found to be governed essentially by the ferritic phase, the good toughness could be ascribed to the presence of austenite that retards the cleavage fracture of ferrite (Ref 1). The intermetallic compounds that nucleate and grow into the ferritic matrix have a detrimental effect on impact toughness, because the particles become hard with structural discontinuities, which, therefore, can act as stress-intensification sites and therefore become the preferential cracking start sites. Therefore, many standards, relating to manufacturing of DSS, require "no intermetallic phases" in the microstructure (Ref 3).

The DSS are submitted to a solution treatment, followed by water quenching, to redissolve the secondary phases formed during the previous processes and to obtain a ferrite/austenite ratio of about one, corresponding to the best mechanical and corrosion properties.

In a previous article (Ref 4), the formation of secondary phases in the UNS S32760 during isothermal treatments, in the temperature range between 850 and 1000 °C has been examined. The results confirmed that the χ phase always appears first at the triple points and at the α/γ interfaces (and sometimes inside the ferritic grains), and is later followed by the σ phase that grows toward the ferrite. This is justified by the lower misfit between the cubic lattice of the χ phase and the parent cubic phase (Ref 1). After long exposition times, the volume fraction of the metastable χ phase is significantly reduced and replaced by the stable σ phase. Thus, it is possible to assert that the χ phase is the metastable precursor of the σ phase, in which χ is gradually transformed (Ref 1). As the results show, both χ and σ phases negatively affect the impact toughness behavior, even if, when both are present, their effects are not distinguishable.

The aim of this study is to investigate the influence of different amounts of intermetallic compounds on the impact toughness behavior, especially in the early precipitation stages. The precipitation of the secondary phases in the microstructure

Irene Calliari, Marco Breda, Emilio Ramous, and **Katya Brunelli**, DPCI, University of Padua, Via Marzolo 9, 35131 Padua, Italy; **Marco Pizzo**, Exova CTR Srl, Via del Santo 211, 35010 Limena (PD), Italy; and **Cinzia Menapace**, DIMTI, University of Trento, Via Mesiano 77, 38123 Trento, Italy. Contact e-mails: irene.calliari@unipd.it; marco.breda@studenti.unipd.it; emilio.ramous@unipd.it; katya.brunelli@unipd.it; marco.pizzo@exova.com; and cinzia.menapace@unitn.it.

has been obtained by means of isothermal aging treatments, carried out at different time-temperature combinations.

2. Experimental

The as-received material was a wrought UNS S32760 SDSS plate ($14.5 \times 1350 \times 6000$ mm), commercially known as Zeron®100, solubilized at 1100 °C and water quenched. The composition of the steel and its mechanical properties are reported in Table 1 and 2, respectively. This steel can be considered as an evolution of the UNS S32750 DSS (SAF 2507), from which the former differs by virtue of the addition of tungsten and a higher amount of copper. Tungsten is added to improve the pitting corrosion, whereas copper increases the wear resistance and the corrosion resistance in sulfuric environments.

The isothermal aging treatments were carried out at 850, 900, and 950 °C for times between 3 and 25 min, as shown in Table 2, and were followed by water quenching. These time-temperature combinations were chosen on the basis of previous results (Ref 4) and after some "preliminary aging treatments," carried out to understand the best minimum aging times for each series.

The different phases detected in the aged samples have been identified by a Cambridge Stereoscan 440 SEM equipped with a Philips PV9800 energy dispersive x-ray spectroscope (EDS) in backscattered-electron mode (29 kV), without etching the specimens. The ferrite appears slightly darker than austenite, while the secondary phases appear lighter. Owing to the higher content of molybdenum, in combination with the large atomic scattering factor of molybdenum, the χ phase appears brighter than the σ phase. In addition, the amount of secondary phases were calculated using an image analysis software, and its determination was performed on the images obtained by SEM-BSE (five fields at ×2000).

The impact toughness has been investigated by means of instrumented impact testing on Charpy V-notched specimens according to the ASTM A 370 specifications for a "minimum average test result" (three $10 \times 10 \times 55$ mm samples for each time-temperature combination) at room temperature and using an available energy of 300 or 150 J (at impact speed of 5.5 or 3.9 m/s, respectively)—note that an impact energy of 150 J has been used for those specimens that certainly would have an absorbed energy lower than 50 J. The load deflection curves were partially smoothed using the moving average method (Ref 5) with a cut-off frequency of 50 Hz.

The fracture surfaces have also been observed by means of SEM, OM, and the stereo-light microscope, to obtain all the necessary information on both the crack nucleation and the fracture propagation, for a macro and microscopic behavior investigation.

Table 1 UNS S32760 material's nominal chemical composition, wt.%

C	Cr	Ni	Mo	Cu	W	Mn	P	S	Si	N
0.014	25.23	6.89	3.67	0.72	0.62	0.88	0.023	0.001	0.25	0.28

Table 2 Most representative specimens

Aging temperature, °C	Aging time, min	Absorbed energy, J	Fracture type	Secondary phases, %
850	5	~300	Ductile	Not present
	8	281	Ductile	Not detected
	10	138	Mixed	0.5
	15	26.5	Mixed	6.2
	25	4.2	Brittle	15.3
900	3	>300	Ductile	Not present
	5	>300	Ductile	Not present
	8	55	Mixed	2.3
	10	56.5	Mixed	2.5
	10	46.5	Mixed	2.5
	15	11.2	Brittle	9.5
950	3	~300	Ductile	Not present
	5	237	Ductile	<0.1
	8	124	Mixed	0.8
	8	99	Mixed	1.2
	15	10.2	Brittle	11.9
	25	4.2	Brittle	15.4

3. Results and Discussion

3.1 Microstructure

Not all the specimens were broken during the impact test: this means that not all the considered aging times have permitted a significant amount of precipitation of intermetallic phases. In fact, as listed in Table 2, the results of the SEM image analysis show that, in some cases, precipitation has not occurred.

The morphology and the localization of the precipitated intermetallic phases are well known and already described (Ref 1, 2). In general, the formation of secondary phases at the grain boundaries and the growth into the ferrite are explained by the diffusion behavior of the elements involved in the transformation: Mo diffusion coefficient is greater than those of Cr, W, and Ni and also greater in ferrite than austenite.

As already reported, in all the considered temperature ranges, the first phase that precipitates is χ, decorating the grain boundaries and the triple points. By increasing the aging time, the volume fraction of χ phase also increases, and the σ phase starts to appear in the form of coarser precipitates at the α/γ boundaries that grow into the ferrite, as shown in Fig. 1. The σ

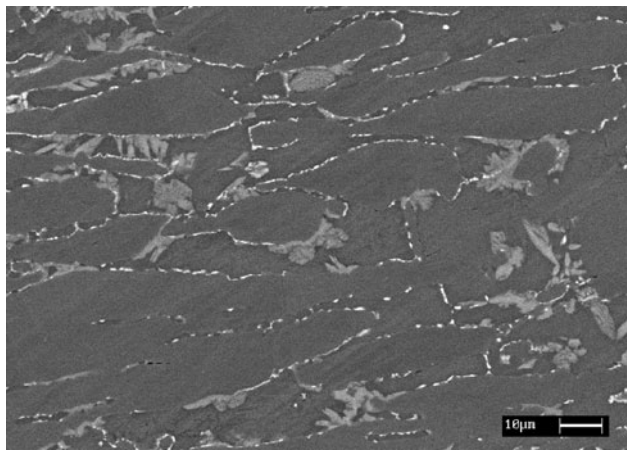

Fig. 1 SEM-BSE image after 15 min at 900 °C with both χ and σ phases

Table 3 EDS analysis, wt.%

Si	Mo	Cr	Ni	W	Fe
α-phase composition in the as received conditions					
0.7	4.8	28.1	5.1	0.7	Bal
α-phase composition after 15 min at 900 °C					
0.8	5.0	28.0	4.4	0.6	Bal
σ-phase composition after 15 min at 900 °C					
0.9	8.6	30.1	4.0	1.4	Bal
χ-phase composition after 15 min at 900 °C					
1.1	10.3	26.1	4.2	2.6	Bal

Note: After 15 min at 900 °C, the amount of secondary phases detected was about 9.5% (comprising 7.9%σ and 1.6%χ)

particles are bigger than χ phase particles and grow more rapidly, embedding some small χ particles: this seems to show the progressive transformation of χ to σ.

Is interesting to note that EDS analyses on both the secondary phases and the parent α-phase compositions have revealed that a large amount of tungsten (also evaluated in the as-received conditions) has passed from the matrix into the intermetallic compounds, and its volume fraction becomes greater in χ rather than in σ (see Table 3). This depletion in tungsten (one of the characterizing elements in this steel) is detrimental for the pitting corrosion resistance and seems to enhance the cracking of the intermetallic phases.

Two factors that cannot be neglected, besides the precipitate's amount, are the distribution and the size of the secondary phases. In fact, it is possible to assert that the impact toughness of the studied material not only depends on the volume fraction of the intermetallic phases but also on the dimension and the distribution of the particles inside the ferritic matrix. The analysis in each of the samples has revealed that the distribution of the secondary phases (pertaining to the same time-temperature combination) is anything but homogeneous. This explains why some specimens, though treated at the same temperature and for the same aging time, exhibit a different impact toughness behavior (even up to 40 J energy difference) and bring out the closer relationship between the impact toughness value and the volume fraction detected closer to the damaged area. The other factor that has to be considered is the size of such particles. Although in this study, an in-depth analysis of the particles size has not been carried out, it is reasonable to assert that, based on the results from a previous study on 2205 DSS (Ref 6), by increasing the aging time, the particles' dimensions also increase, resulting in an ever more pronounced embrittling effect.

3.2 Impact Toughness

As previously reported, not all the tested specimens were completely broken. For a few of them (18 samples out of 45 tested), the absorbed energy was over 300 J or around this value: this means that the aging time was not enough to allow for the precipitation of the intermetallic phases or to allow for their precipitation of a significant amount, to enable it to compromise the impact toughness. As expected, these are the specimens treated for the shorter times, and hence, we were not able to estimate their average absorbed impact energy.

In Fig. 2, the impact energy of the materials under study is shown as a function of their contents in intermetallic phases. The effect of the secondary phases is evident starting from

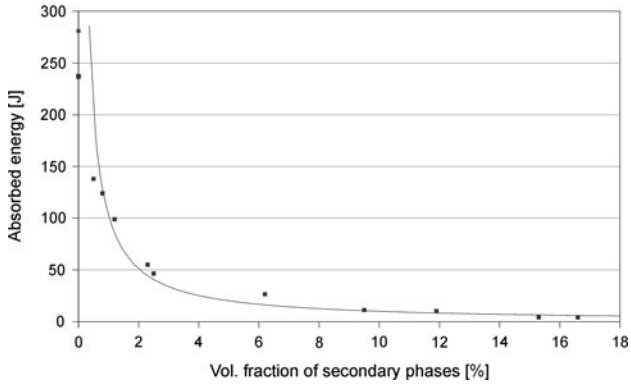

Fig. 2 Impact energy as function of contents in intermetallic phases

0.5% volume fraction for which the impact energy was about 140 J (this means a reduction on impact toughness by over 50%). A further reduction can be seen for 1% volume fraction of intermetallic phases, for which the impact toughness was about 100 J, and a final reduction is registered for amounts over 1.5-2%, for which the registered impact toughness is around 50 J, and small entities of plastic deformations are enough to cause prevailing brittle fracture mechanism. These results agree with some DSS specifications, requiring an intermetallic phase content about $<1\%$, to assure a minimum impact energy of 40-50 J (Ref 3). The relation between the impact energy and the contents of volume fraction of secondary phases is evident: a very low content is enough to produce very dangerous effects. By increasing the precipitates' amounts, the fracture mechanism shows an ever more prominent brittle behavior until 6% volume fraction, exceeding which the ductile component is totally absent.

The results shown in the figure suggest subdivision of the examined samples in three regions on the basis of the fracture energy values. To each region correspond a different shape of the load deflection curve and a different fracture behavior, as reported in Fig. 3(a)-(d). Obviously, the boundaries between the three regions are not well defined, and the materials' behaviors show a gradual transition from the completely ductile to completely brittle fracture mechanism.

Before discussing the subdivision of the graph in Fig. 2, it is interesting to note that the specimens with a registered absorbed impact energy >300 J were not completely broken (i.e., the available energy in the impact was totally absorbed by the samples without causing the complete rupture), no secondary phases were detected, and for these specimens, the fracture was completely ductile. For these specimens, we can establish that, the aging time, at the considered temperature, was not enough to allow for a significant intermetallic precipitation. A similar behavior was noted in the specimens broken with an impact energy around 300 J.

The materials with an impact energy >160 J, characterized by a content of intermetallic phases $<0.5\%$, pertain to the first region. From Fig. 3(a) (sample aged at 950 °C for 5 min), it is seen that, after the general yielding at about 20 kN, the applied load initially increases because of strain hardening, and the fracture nucleates in relation to the maximum load and is followed by a stable crack propagation, because of the ductile mechanism. The microstructural analysis has revealed a small amount of secondary phases, identified as mainly χ phase. It is easily noted that, with an increase of the intermetallic amount, the absorbed energy is ever lower and the fracture behavior is

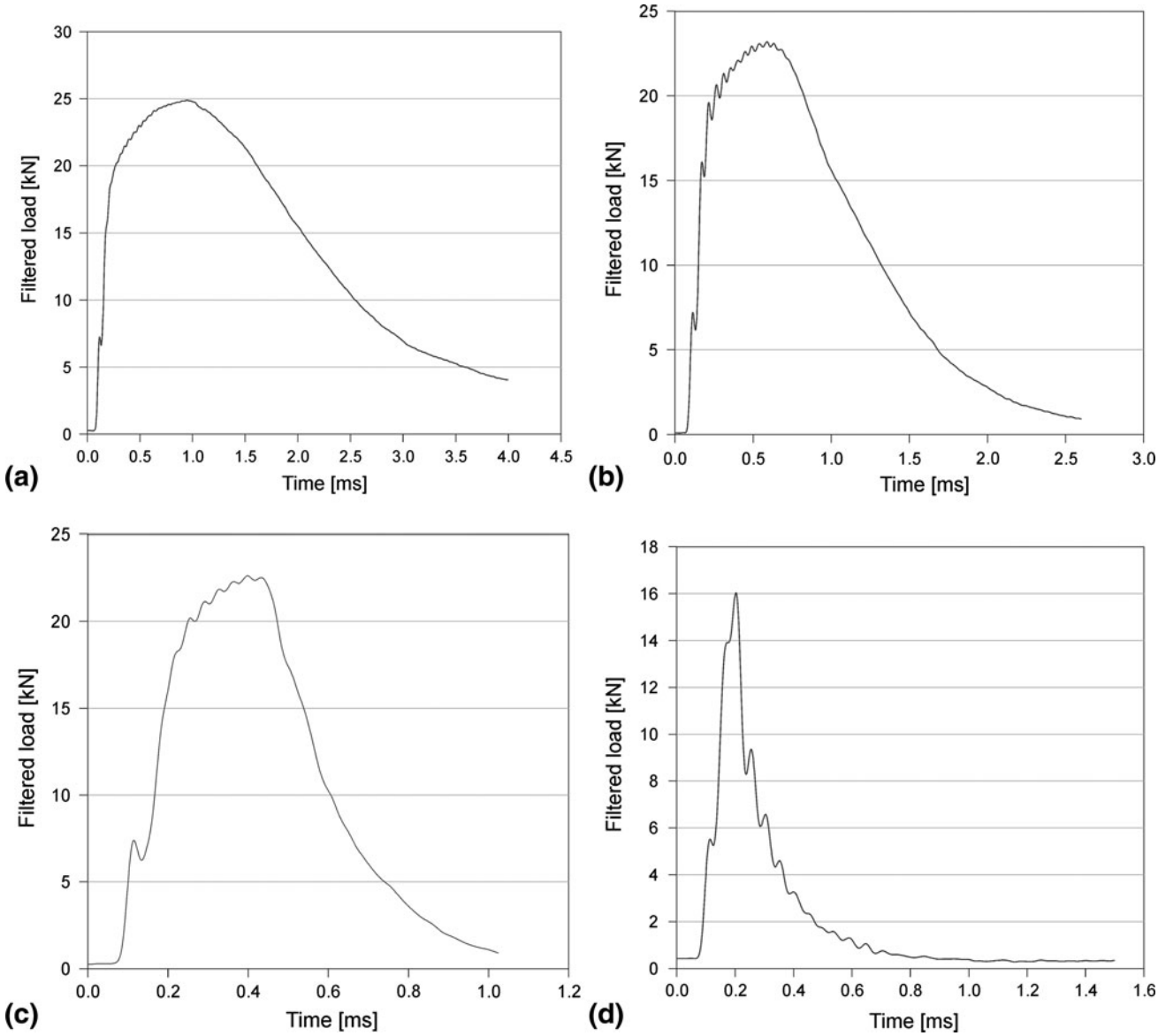

Fig. 3 (a) Impact curve of sample with impact energy >160 J (950 °C for 5 min). (b) Impact curve of sample with impact energy 60-160 J (850 °C for 10 min). (c) Impact curve of sample with impact energy <60 J in the first sub-region (900 °C for 8 min). (d) Impact curve of sample with impact energy <60 J in the second sub-region (900 °C for 15 min)

ever more brittle, resulting in a change in the curve slope after the maximum load and in a reduction of the fracture propagation time.

The materials with an impact energy between 60 and 160 J pertain to the second region, for which the content of intermetallic phases is between about 0.5 and 1.5%. For these specimens, the fracture behavior is not completely ductile: this is confirmed by the impact curve shown in Fig. 3(b) for a sample aged at 850 °C for 10 min. By analyzing the impact curve, it can be noted that, after the general yielding that still occurs at about 20 kN, the material undergoes strain hardening, and the ductile fracture nucleates at the maximum load. The curve shows that, after a stable crack propagation, the brittle mechanism takes place, causing a marked change in the impact curve slope and reduction in the absorbed energy. The entity of the brittle component is related to the amount of the precipitates and is more prominent in the specimens where it increases. The brittle behavior can obviously be associated to the rupture of the hard intermetallic phases and to the crack propagation into the adjacent ferritic phase. Microstructural analysis has revealed the presence of both σ and χ phases.

Materials with an impact energy <60 J, characterized by a content of intermetallic phases >1.5%, pertain to the third region. This region can be subdivided into two sub-regions: although in the whole region, the fracture is prevailingly brittle, it becomes completely brittle for amounts of secondary phases >6%. For an intermetallic amount between 1.5 and 6%, an ever smaller ductile component has been observed, till its complete disappearance for intermetallic amounts that exceed the latter value of precipitation. Thus, the first sub-region refers to those materials that present an intermetallic content between 1.5 and 6%, and the related curves are shown in Fig. 3(c). On the other hand, those materials that show a completely brittle behavior pertain to the second sub-region (see Fig. 3d). In both

sub-regions, a microstructural analysis revealed the presence of both σ and χ phase, with an amount of σ much more prominent.

For the materials in the first sub-region, the general yielding still occurs at 20 kN, but for shorter times. After the yielding at the notch root, the brittle fracture takes place, resulting in rapid fracture propagation and in low energy absorption. We can assert that a small amount of plastic deformation at the notch root is enough to reach the critical brittle fracture conditions. Furthermore, the hard secondary phases allow an easier crack nucleation and contribute to determining an energy-favored path for the crack propagation. The curves for these materials also show that the intermetallic amount has no influence on the general yielding value and on the overall yielding behavior, even if it occurs for shorter times when the strain hardening contribution is smaller.

For the materials in the second sub-region, the fracture behavior is completely brittle, and no (or very slight) plastic deformations at the notch root have been observed. With these amounts of precipitates, the impact toughness is totally compromised and also the yielding behavior is modified, resulting in a progressive decrease of the general yielding value and in a progressive disappearance of the strain hardening.

3.3 Correlations

With the obtained data, we can estimate the fracture toughness (K_{mat}) of the steel under study for a (partial) structural integrity assessment. Although the tests were not carried out with a direct dependence from the temperature (i.e., the tests were all performed at room temperature after the aging treatments), the material shows a ductile-to-brittle transition that is somehow possible to relate to the transition obtained by decreasing the test temperature. In fact, even though the shape of the obtained curve is not similar to the transition temperature trend, the materials exhibit a gradual decrease of the impact toughness because of the ever more damaged microstructure, which is similar to the decrease in ductility when the temperature is lowered. Thus, it is possible to relate the material's behavior to the so-called Master Curve Approach where the secondary phases, randomly distributed inside the microstructure, can be associated to low toughness regions as in the "weakest links" hypothesis (Ref 7).

For the ductile regime ($KV > 160$ J in the present study), the correlation between the Charpy data (KV) and the fracture toughness is given by (Ref 8)

$$K_{mat} = (0,54)\, KV + 55$$

resulting in a conservative prediction.

Although the previous equation is recommended when the Charpy energy is greater than 60 J, it is not usable for the transition regime in the present study (160 J $< KV <$ 60 J) because of the presence of the brittle mechanism that begins to manifest itself in an ever more pronounced manner. Furthermore, the so-called Master Curve Equation, suitable for the transition regime, is not even usable because a real transition temperature does not exist in this study (the method needs the definition of the "Charpy 27 J temperature"), and so the equation should be rearranged for the specific case.

Finally, for the brittle regime ($KV < 60$ J in the present study), the correlation could be given by (Ref 8)

$$K_{mat} = 12\sqrt{KV}$$

$$K_{mat} = \left[(K_{mat25} - 20)\left(\frac{25}{B}\right)^{\frac{1}{4}}\right] + 20$$

where the estimated fracture toughness of the material, K_{mat25}, must be corrected for the appropriate thickness B.

It is worthwhile to take note of the Charpy 27 J critical impact toughness value: this value is relevant to materials' testing standards which frequently require a minimum Charpy impact energy of 27 J. In Ref 1 the TTT diagram for SAF 2507 with the curve corresponding to 27 J, impact toughness has been reported. In the present study, a full analysis on the effects of the isothermal treatments on the impact toughness in the whole temperature range of 700-1000 °C has not been done, but is it reasonable to say something about the time-temperature combinations that allow for a significant precipitation's amount, which leads to an impact toughness value about 27 J. From the impact test results, it can be seen that the critical value of secondary phases is reached after aging the material at 850 °C for 15 min, while for the other two temperatures, we can only state that the critical value is reached between 10 and 15 min after aging at 900 °C, and between 8 and 15 min if the material is treated at 950 °C.

3.4 Fractography

From the examination of the fracture's morphology and from the microstructural analysis closer to the damaged area, we were able to relate the influences of the secondary phases on the deformation and fracture behavior of the tested materials.

The materials in the first region show a ductile behavior, and the fracture occurs after a large plastic deformation; the morphology is ductile and shows the characteristic dimpled surface, as seen from Fig. 4. Nevertheless, the occurrences of some micro-voids at the triple points and at the grain boundaries near the fracture surface have been observed, probably because of the original presence of small intermetallic particles. The presence and the nature of these particles greatly influence the initiation of micro-cracks, because they crack during the deformation and act as ductile fracture nucleation sites.

The third region comprises those materials that failed in a brittle manner. For these materials, the damaged region close to the notch root is characterized by the presence of a large number of micro-cracks in relation to the secondary phases; a fracture morphology analysis has revealed the presence of cleavage and quasi-cleavage facets in the fracture surface (see Fig. 5 and 6). For the materials in the third region, the density of such micro-cracks is high, because of the large contents of the secondary phases, and in addition, their larger sizes. The brittle fracture occurs quite early, following a very small plastic deformation at the notch root, sufficient to reach the critical value.

For the materials of the second region, the critical conditions at the notch root for the brittle fracture nucleation are reached after a large plastic deformation. The densities and the sizes of the micro-cracks are lower than in the case of materials in the third region, because of the lower amount of embrittling secondary phases. However, this is a transient region, and so the behavior of the material changes when considering the upper and the lower energy limits, showing an ever more brittle fracture mechanism and an ever lower plastic deformation as

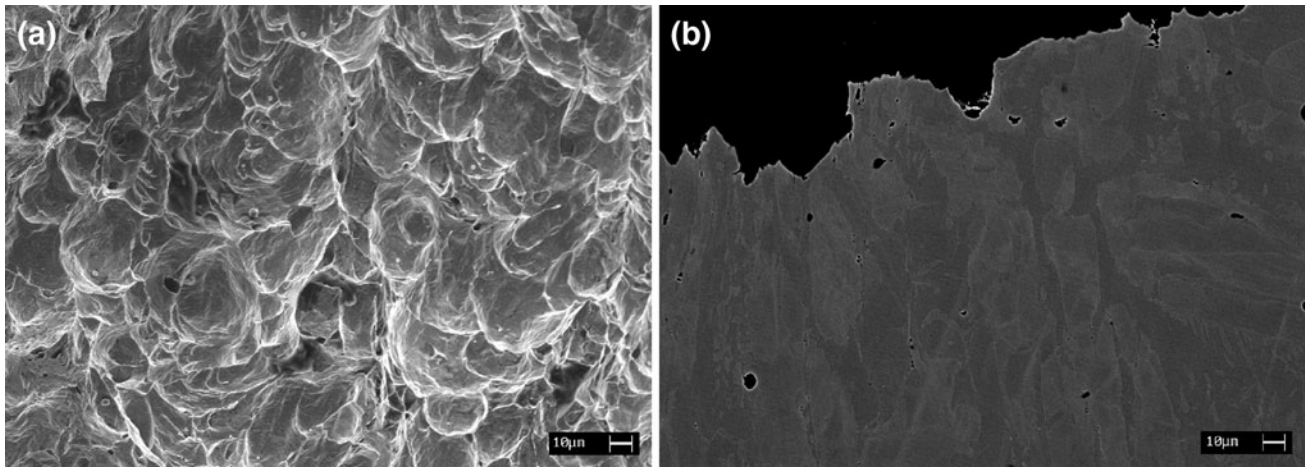

Fig. 4 (a) SEM-SE image of fracture surface (sample failed at 237 J). (b) SEM-BSE image of cross section close to notch root (sample failed at 237 J)

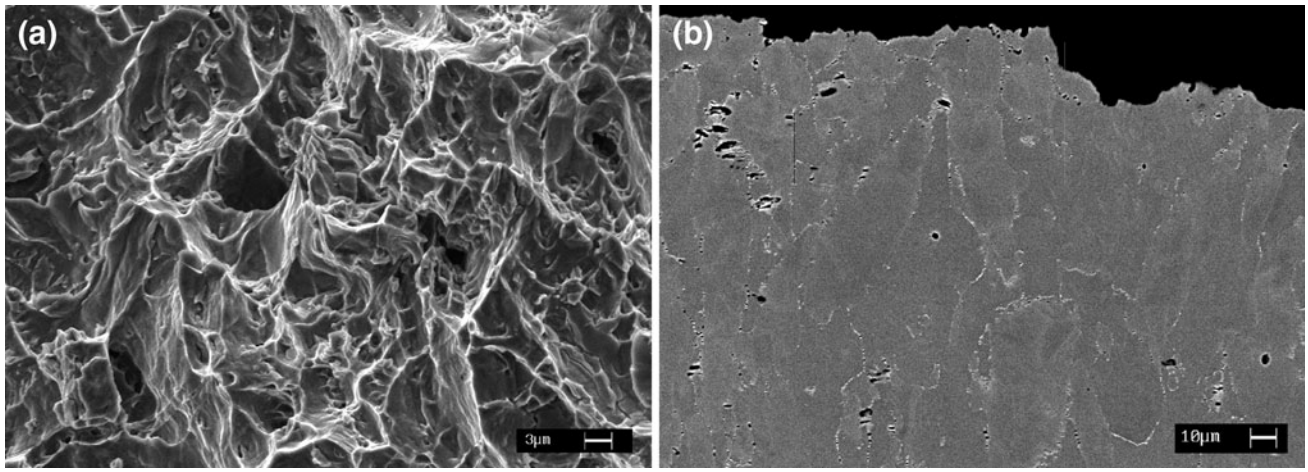

Fig. 5 (a) SEM-SE image of fracture surface (sample failed at 55 J). (b) SEM-BSE image of cross section close to notch root (sample failed at 55 J)

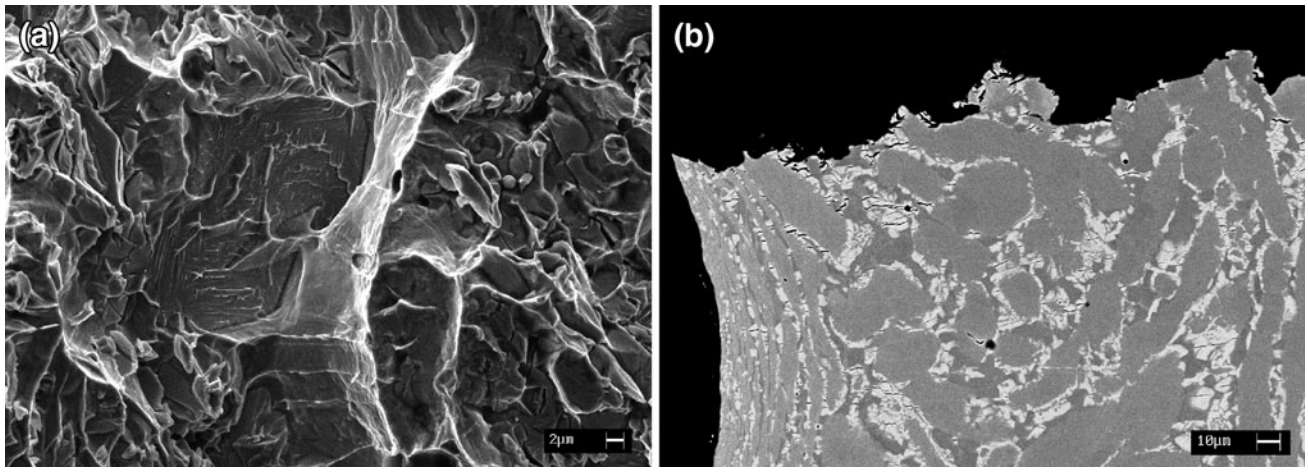

Fig. 6 (a) SEM-SE image of fracture surface (sample failed at 4.2 J). (b) SEM-BSE image of cross section close to notch root (sample failed at 4.2 J)

the intermetallic amount increases. Thus, the fracture surface morphology exhibits the characteristic features of both brittle and ductile nature (dimples and cleavage facets), shifting toward either the former or the latter depending on amounts of the secondary phases.

4. Conclusions

The effect of the isothermal treatment in the temperature range 850-950 °C on the impact toughness of UNS S32760 super DSS can be summarized as follows:

1. During the aging treatments, the χ phase is the first intermetallic phase that precipitates, always at the α/γ boundaries and at the triple points; it is followed by the σ phase that gradually becomes embedded and eventually replaces the former.
2. For the samples with a volume fraction of intermetallic compounds of about 0.5%, the absorbed energy is reduced by over 50%.
3. The effect of secondary phases on the impact toughness becomes already evident starting from amounts $<0.5\%$. In this case, the impact energy is lower than 160 J, the fracture is ductile, and the secondary phases contribute to crack nucleation.
4. Another reduction in impact toughness is observed for intermetallic amounts between about 0.5 and 1.5%, and the associated absorbed energy is lower than 160 J. In these samples, the critical conditions for the brittle fracture nucleation are reached after a large plastic deformation and, after a stable crack propagation of the brittle mechanism takes place. Nevertheless, the results show that the materials present an ever more brittle fracture mechanism and an ever lower plastic deformation as the intermetallic amount increases.
5. If the intermetallic amount is $>1.5\%$, then a great reduction in impact toughness is observed. The region can be subdivided into two sub-regions, and the limit between the two can be positioned at about 6% of intermetallic amount. In the first sub-region, a low amount of plastic deformation is enough to reach the critical brittle fracture conditions, but this has no influence on the general yielding value. For the materials in the second sub-region, the impact toughness is totally compromised, and both the yielding behavior and the fracture time are greatly reduced, as well.
6. The results of the investigation show that both χ and σ phases negatively affect the impact toughness behavior, when both are present, even if their effects are not distinguishable.
7. It can also be asserted that the impact toughness of the studied materials depends not only on volume fractions of their intermetallic phases but also on their dimension and their distribution inside the ferritic matrix.
8. With these experimental data, we are able to obtain some useful correlations between the Charpy's values of impact toughness and the fracture toughness K_{IC} on the basis of the empirical relations introduced in Ref 8.

Acknowledgments

The authors would like to thank Eng. G. Straffelini from the *DIMTI of University of Trento*, Mr. M. Baldan from *Exova C.T.R. Srl,* and all those from the *DPCI of University of Padua,* who have contributed to this study.

References

1. J.O. Nilsson, Overview: Duplex Stainless Steels, *Mater. Sci. Technol.*, 1992, **8**, p 685–700
2. R.N. Gunn, *Duplex Stainless Steels: Microstructure, Properties and Applications*, R.N. Gunn, Ed., Abingdon Publishing, Cambridge, 1997, p 1–15
3. R.B. Johansen, B.H. Leinum, S. Karlsen, H.A. Trandem, G. Valdø, A.O. Tjernæs, and T. Helgesen, Duplex Stainless Steels—Measurement of Intermetallic Phase Content and the Connection to Impact Toughness and Corrosion Resistance, *Proceedings of the Conference on Duplex 2000*, October 2000 (Venice, Italy), AIM, 2000, p 405–412
4. I. Calliari, M. Pellizzari, and E. Ramous, Precipitation of Secondary Phases in Super Duplex Stainless Steel Zeron®100 Isothermally Aged, *Mater. Sci. Technol.*, 2011, **27**, p 928–932
5. G. Straffellini, Impact Fracture Toughness of Porous Iron and High-Strength Steels, *Metal. Mater. Trans. A*, 2000, **31A**, p 1443–1451
6. I. Calliari, G. Straffellini, and E. Ramous, Investigation of Secondary Phase Effect on 2205 DSS Fracture Toughness, *Mater. Sci. Technol.*, 2010, **26**, p 81–86
7. K. Wallin, Innovative Approaches to Irradiation Damages and Fracture Analysis, 1989, **170**
8. A.C. Bannister, "Structural Integrity Assessment Procedures for European Industry (SINTAP)—Sub-Task 3.3 Report: Determination of Fracture Toughness from Charpy Impact Energy: Procedure and Validation", Document No. SINTAP/BS/15. British Steel plc., 1997